

Alternative evaluations of halos in nuclei

S. Karataglidis^(a), P. J. Dortmans^(b), K. Amos^(b), and C. Bennhold^(c)

^(a) *TRIUMF, 4004 Wesbrook Mall, Vancouver, British Columbia, V6T 2A3, Canada*

^(b) *School of Physics, University of Melbourne, Parkville, Victoria, 3052, Australia*

^(c) *Center of Nuclear Studies, Department of Physics, The George Washington University,
Washington, D.C., 20052*

(March 27, 2022)

Abstract

Data for the scattering of ${}^6\text{He}$, ${}^8\text{He}$, ${}^9\text{Li}$, and ${}^{11}\text{Li}$ from hydrogen are analyzed within a fully microscopic folding model of proton-nucleus scattering. Current data suggest that of these only ${}^{11}\text{Li}$ has a noticeable halo. For ${}^6\text{He}$, we have also analyzed the complementary reaction ${}^6\text{Li}(\gamma, \pi^+){}^6\text{He}_{gs}$. The available data for that reaction support the hypothesis that ${}^6\text{He}$ may not be a halo nucleus. However, those data are scarce and there is clearly a need for more to elicit the microscopic structure of ${}^6\text{He}$.

I. INTRODUCTION

Much information has been learned concerning the nature of halos in nuclei from studies of heavy ion break up reactions in which the momentum distributions of the valence nucleons have been found to be very narrow [1]. This observation suggests matter distributions which extend well beyond the radius of the nuclear potential and examples of halos found by this means are ^{11}Li and ^{11}Be . Different neutron distributions in exotic nuclei, such as skins (^8He , for example), also have been studied using this method. However, doubt remains on the ability of such reactions to probe the initial state wave functions. The breakup of ^6He has been demonstrated to be a two-step process [2], in which the ^5He fragment survives for a considerable amount of time as an $\alpha - n$ resonance before it breaks up. This suggests that the effects of final state interactions are significant in this reaction, so that information concerning the initial state wave function is lost.

Also, that approach has the disadvantage of missing part of the initial state wave function of the halo nucleons [3] probing only the asymptotic part of the wave function. Success has been achieved in the analysis of those reactions using few-body models for the halo nuclei (see Ref. [4] and references therein) as they are able to describe the asymptotic parts of nuclei better than most shell models [5]. There remains the need to find ways of studying microscopic properties of the wave functions of halo nuclei.

To study the microscopic aspects of the wave functions of exotic nuclei we look to alternatives which probe the entire wave function. Proton scattering in the inverse kinematics and charged pion photoproduction are such reactions. Experiments have been performed for the (elastic) scattering of radioactive ions from hydrogen (see, for example, [6]). In the inverse kinematics this corresponds to proton scattering from the heavy ion, which directly measures the matter distribution of that ion. In particular, depending on the momentum transfer, such scattering may measure the density near the surface of the nucleus so that detailed information on the halo may be collected. Charged pion photoproduction from nuclei may serve as a useful complementary probe of halo structures [7], especially as that reaction also is sensitive to the entire halo wave function formed in the final state. We present analyses of data on both of these reactions to study the neutron distributions of ^6He , ^8He , ^9Li , and ^{11}Li to determine whether the results permit identification of any of these nuclei as a neutron halo or neutron skin system.

II. MODELS OF STRUCTURE

As both proton scattering and charged pion photoproduction reactions probe the microscopic structure of the nucleus, a suitable model for the description of halo nuclear states in those reactions would be one in which nucleon degrees of freedom are admitted. This would, by necessity, include the core. In the case of ^{11}Li scattering from hydrogen, it was found that a full description of the ^9Li core was required [8] to describe the elastic scattering data. Therefore, we describe the halo states within the shell model, and allow for all nucleons to be active within the space (the so-called “no-core” models).

Several groups report shell model calculations of $^{6,8}\text{He}$ and $^{9,11}\text{Li}$. Navrátil and Barrett [9,10] have made large-space shell model calculations using interactions obtained directly from the NN g matrices, with the Reid93 NN interaction as their base. Their calculations

for ${}^6\text{He}$ were made in a complete $(0 + 2 + 4 + 6)\hbar\omega$ model space while those for ${}^8\text{He}$, ${}^9\text{Li}$ and ${}^{11}\text{Li}$ were made in the smaller $(0 + 2 + 4)\hbar\omega$ model space; the limitation arising from the dimensionality increasing with mass for a given space. (Henceforth, only the highest excitation will be given in reference to the complete model space.) Good results were found for the ground state properties in each case. For ${}^6\text{He}$, specifically, their calculations indicate that there is little or no need for this system to have a neutron halo to obtain agreement. For the other nuclei, they find spectra and ground state properties that are also quite good, although the calculated proton root-mean-square (r.m.s.) radii are small in comparison to the measured values. The cause of these discrepancies may be a halo-like distribution of the excess neutrons; the $4\hbar\omega$ model space is not large enough to admit such halo characteristics for these nuclei [10]. These calculations may be contrasted with the results of our recent study [11] in which the results of $0\hbar\omega$ and $2\hbar\omega$ shell model calculations of ${}^9\text{Li}$ and ${}^{11}\text{Li}$, made using phenomenological interactions, were reported. When using the wave functions obtained in those smaller space calculations, the available elastic scattering data at $60A$ and $68A$ MeV from hydrogen were well described.

We have calculated the wave functions for ${}^{6,8}\text{He}$ within a complete $4\hbar\omega$ model space using the G matrix interaction of Zheng *et al.* [12]. For ${}^{9,11}\text{Li}$, we used the wave functions as calculated in our previous work [11]: using the P(5–16)T interaction in the $0\hbar\omega$ model space for ${}^9\text{Li}$, and the WBP interaction [13] in the $2\hbar\omega$ model space for ${}^{11}\text{Li}$. All calculations were made using the shell model code OXBASH [14]. From those wave functions, the one-body density matrix elements (OBDME) were obtained to use in the descriptions of the scattering and of the (γ, π^+) reaction.

The spectrum of ${}^6\text{He}$ is displayed in Fig. 1. Therein, the results of our calculation are compared to those of the $6\hbar\omega$ calculation of Navrátil and Barrett [9], as well as to those of Pudliner *et al.* [15], in which the spectra of $A = 6$ nuclei were calculated using the Variational Monte Carlo (VMC) shell model approach. The experimental spectrum was obtained from Ref. [16]. The two calculations made using the “traditional” shell model approach ascribe $J^\pi; T = 2^+; 1$ to the first two excited states, in agreement with experiment. While the energy of the $2_1^+; 1$ state is similar in the $4\hbar\omega$ and $6\hbar\omega$ models, the energy of the 2_2^+ state in the $6\hbar\omega$ model is in much better agreement with the data. This may be due to the modification of the auxiliary potential in the Hamiltonian in that calculation [9]. Without that modification, overbinding is observed, of the order of 4 MeV. However, it does not affect the spectrum significantly; the increase in energy of each state is less than 1 MeV. It should be noted that this overbinding will also affect our calculations, as we use the same interactions, although we do not expect that the wave functions will be significantly affected. The results of the VMC calculation place the 2_1^+ state in very close agreement with experiment. However, that calculation also has an extra 1^+ state in the spectrum not observed, nor seen in the other calculations. It would be interesting to investigate in more detail the character of that particular state.

There is very little experimental information on the spectrum of ${}^8\text{He}$. The first excited state is listed at 2.8 ± 0.4 MeV and has $J^\pi; T = (2^+); 2$ [17]. Other states are reported at 1.3, 2.6 and 4.0 MeV [17], as obtained from a transfer experiment involving heavy ions, but no other data are available as yet to support those measurements. The results from the present calculation are compared to those obtained from the VMC calculation [18] in Fig. 2. The spectrum obtained by Navrátil and Barrett in the $4\hbar\omega$ model space using their updated

G matrix interaction [10] is similar to the present results, and so are not shown. The $2_1^+; 2$ state is predicted correctly by all calculations as the first excited state, although only the VMC calculation agrees well with experiment. The disagreement between the shell model calculations and experiment may be due to the shell model failing to reproduce, within the $4\hbar\omega$ model space, the correct neutron density distribution. ^8He has a well-known neutron skin, the description of which may require a calculation using a very large model space.

The ^9Li spectrum is displayed in Fig. 3, wherein the results of the present calculation are compared to those obtained within the $4\hbar\omega$ model space. The experimental energies are obtained from [17]. The spectrum obtained in the $0\hbar\omega$ model space is in general agreement with that obtained in the $4\hbar\omega$ model space, although the first excited state comes much lower in the latter. There are no spins assignments in the experimental spectrum bar the ground and first excited states, which the models correctly predict. As we consider only the elastic channel in the calculations of proton scattering, the $0\hbar\omega$ calculation is sufficient. One expects that core polarization corrections will become important for inelastic scattering.

The ^{11}Li spectrum is displayed in Fig. 4. Therein, the experimental results of Gornov *et al.* [19] are compared to the results of the present calculation. The experiment from which the excitation spectrum was obtained was $^{14}\text{C}(\pi^-, pd)^{11}\text{Li}$ and did not allow for any spin assignments to be made so the comparison between experiment and theory at this stage must be tentative. The $\frac{1}{2}_1^-; \frac{5}{2}$ state is formed from the coupling of the valence neutrons to the $\frac{1}{2}^-$ state in ^9Li .

III. ELASTIC PROTON SCATTERING

We now consider elastic scattering of the heavy ions from hydrogen, data for which are available at 72A MeV for $^6,^8\text{He}$ and 62A MeV for $^9,^{11}\text{Li}$. The analyses follow those made for the elastic scattering of 65 MeV protons from various targets ranging from ^6Li to ^{238}U [20], and we refer the reader to that reference for complete details. We present a brief summary of the formalism herein.

There are three essential ingredients one must specify to calculate proton scattering observables. The first are the OBDME as obtained from the shell model calculations. They are explicitly defined as

$$S_{\alpha_1\alpha_2I} = \left\langle J_f \left\| \left[a_{\alpha_2}^\dagger \times \tilde{a}_{\alpha_1} \right]^I \right\| J_i \right\rangle \quad (1)$$

where J_i and J_f are the initial and final nuclear states respectively, I is the angular momentum transfer, and $\alpha_i = \{n_i, l_i, j_i, \rho_i\}$ with ρ specifying either a proton or a neutron.

The second ingredient is the effective interaction between the projectile nucleon and each and every nucleon in the target. The complex, fully nonlocal, effective interaction we choose [20] accurately maps onto a set of nucleon-nucleon (NN) g matrices. These density-dependent g matrices are solutions of the Brueckner-Bethe-Goldstone equations in which a realistic NN potential defines the basic pairwise interaction. For that, we have chosen the Paris interaction [21]. Good to excellent predictions of the elastic scattering observables for stable targets from ^6Li to ^{238}U were found with this effective (coordinate space) interaction.

Finally, the single particle wave functions describing the nucleon bound states must be specified. For the present calculations we distinguish between those calculations which yield

an extensive (halo) density distribution and those that do not. The former we designate “halo” while the latter are designated “non-halo”. Those calculations use single-particle wave functions as specified naively from the shell model calculations, which do not make allowance directly for the very loose binding of the valence neutrons, at least not to the level in $\hbar\omega$ assumed in the model spaces. In all cases bar one, Woods-Saxon (WS) wave functions were used. Those which gave good reproduction of the elastic electron scattering form factors of ${}^6\text{Li}$ [5] were used for all the ${}^{6,8}\text{He}$ calculations while those which reproduced the elastic electron scattering form factors of ${}^9\text{Be}$ [23] were used in the calculations for ${}^9\text{Li}$, and also for the core in the halo calculation of ${}^{11}\text{Li}$. For the non-halo specification of ${}^{11}\text{Li}$, we used appropriate harmonic oscillator wave functions for mass-11 [11]. To specify the halo, we adjusted the WS potentials from the values given such that the relevant valence neutron orbits are weakly bound. Those are the $0p$ -shell orbits and higher for the helium isotopes, and the $0p_{\frac{1}{2}}$ orbit and higher for the lithium ones. Such an adjustment to single particle wave functions adequately explains the very large $B(E1)$ in ${}^{11}\text{Be}$ [24] and guarantees an extensive neutron distribution. In our analyses, ${}^8\text{He}$ and ${}^9\text{Li}$ act as controls: ${}^8\text{He}$ is an example of a neutron skin and ${}^9\text{Li}$ is a simple core nucleus. The single neutron separation energies are 2.137 MeV and 4.063 MeV for ${}^8\text{He}$ [17] and ${}^9\text{Li}$ [22], respectively. We may artificially ascribe a halo to these nuclei, by setting a much lower separation energy, to ascertain if the procedure and data are sensitive enough to detect the flaw. For ${}^6\text{He}$, the $0p$ -shell binding energy was set to 2 MeV, which is close to the separation energy (1.87 MeV [17]) of a single neutron from ${}^6\text{He}$, leaving the lowest $0p$ -shell resonance in ${}^5\text{He}$. For ${}^8\text{He}$, ${}^9\text{Li}$ and ${}^{11}\text{Li}$, the halo was specified by setting the binding energy for the WS functions of the $0p_{\frac{1}{2}}$ and higher orbits to 0.5 MeV [11]. While the halo and nonhalo specifications are a matter of convenience at this point, we test the validity of halo name by calculating the r.m.s. radii for all four nuclei.

The ability by which the wave functions can describe halo states may be evaluated by calculating the r.m.s. radius for each nucleus and compare to those results obtained from analyses of the reaction cross sections. The r.m.s. radii are presented in Table I, as calculated using the shell model wave functions and the specified single particle wave functions. The values obtained from the shell model using the correct single particle wave functions are largely consistent with those obtained from few-body calculations [25–27]. The values obtained indicate that ${}^6\text{He}$ and ${}^{11}\text{Li}$ are halo nuclei, while ${}^8\text{He}$ and ${}^9\text{Li}$ are not. While our prediction for the r.m.s. radius for ${}^{11}\text{Li}$ appears lower compared to the value extracted from the reaction cross section [26], it is consistent within the error bars quoted with that analysis. The lower value may be due to the wave functions possibly being incapable of describing long range phenomena adequately. If that is the case, more $\hbar\omega$ excitations must be admitted into the model space; although the present set of wave functions should be sufficient to describe the proton scattering observables at high momentum transfer.

The calculations for the scattering from ${}^9\text{Li}$ and ${}^{11}\text{Li}$ are those presented in Ref. [11], while those for ${}^6\text{He}$ and ${}^8\text{He}$ used the OBDME as we have obtained from our shell model wave functions.

The neutron density profiles for ${}^6\text{He}$, ${}^8\text{He}$, ${}^9\text{Li}$, and ${}^{11}\text{Li}$ obtained from the present shell model calculations are shown in Fig. 5. Therein the dashed and solid lines portray, respectively, the profiles found with and without the halo conditions being implemented. The dot-dashed line in each case represents the proton density. As the folding process defines

the optical potentials, the internal ($r < r_{\text{rms}}$) region influences the predictions of differential cross sections, notably at large scattering angles. In this region the extensive (halo) distribution exhibits a lower density, as the neutron strength is bled to higher radii. That effect characterized the proton halo in $^{17}\text{F}^*$ as manifest in the $^{17}\text{O}(\gamma, \pi^-)$ reaction [7]. The extended nature of the halo also influences the optical potentials as evidenced in changes to the cross sections at small momentum transfers (typically $< 0.5 \text{ fm}^{-1}$ or $\theta_{c.m.} < 15^\circ$ for beam energies between $60A$ and $70A$ MeV).

The predicted differential cross sections for the scattering of $^{6,8}\text{He}$ and $^{9,11}\text{Li}$ from hydrogen are presented in Figs. 6 and 7. In Fig. 6 we display the results to 80° ($q \sim 2.5 \text{ fm}^{-1}$) and compare them with the data taken by Korshennikov *et al.* [6,30] using $70.5A$ MeV ^6He and $72A$ MeV ^8He beams, and by Moon *et al.* [31] using $60A$ MeV ^9Li and $62A$ ^{11}Li beams. The forward angle results specifically, for which there are no data, are shown in Fig. 7 to emphasize the influence on the predictions by the extension of the halo ($r > r_{\text{rms}}$). In both figures the solid curves depict the non-halo results while the dashed curves are those with the halo.

As is evident in Fig. 6, the data for our two controls, ^8He and ^9Li , are sufficient to resolve the question of whether these nuclei exhibit halos. In both cases the data above 50° are reproduced by the non-halo results suggesting that these nuclei do not have extended (halo) neutron distributions. This gives confidence in our ability to use such data to determine if a nucleus has a halo. That is confirmed in the case of the scattering of ^{11}Li from hydrogen as the data clearly support a halo structure. There are differences evident between the halo and the non-halo predictions with these nuclei when one considers small angle scattering, where the influence of the Coulomb interaction is quite important. We present the results of our calculations for small angle scattering in Fig. 7. For ^9Li , the difference between the halo and non-halo results is small which supports the notion that this nucleus is a close-packed system. This is contrasted by the results for both ^8He and ^{11}Li : the difference between the halo and non-halo results for ^{11}Li is greater, suggesting again the halo structure, but the difference is greatest in ^8He . Together with the large angle scattering data this suggests the neutron skin structure for ^8He serves to dilute the charge distribution stemming from the two protons while pushing the density of the neutrons uniformly to larger radii as is shown in Fig. 5.

We now turn our attention to ^6He . As shown in Fig. 6, the existing ^6He data range only to 50° ($q \sim 1.6 \text{ fm}^{-1}$). This is insufficient to discriminate between the halo and non-halo structures. As confirmed by the data and optical model analysis of Korshennikov *et al.* [6], our results are almost identical to those from p - ^6Li scattering, but only in the region where the data were taken for the p - ^6He scattering. Beyond this region there is a sufficient difference between the calculations to determine if ^6He exhibits a halo. Data are needed beyond 50° to make such an assessment. The small angle scattering shown in Fig. 7 is consistent with the result for ^9Li in showing little difference between the halo and non-halo results.

We may also study ^6He via the $^6\text{Li}(\gamma, \pi^+)^6\text{He}_{gs}$ reaction. This reaction may be more sensitive to details of the halo as the transition is more sensitive to the descriptions of the valence neutrons. We have calculated the cross sections for this reaction at $E_\gamma = 200$ MeV using the DWIA model of Tiator and Wright [32]. As the ^6He ground state is the isobaric analogue of the $0^+; 1$ (3.563 MeV) state in ^6Li , we have used the OBDME for the transition

to that state in ${}^6\text{Li}$, as obtained from a complete $(0 + 2 + 4)\hbar\omega$ shell model calculation [5]. The non-halo result corresponds to a calculation using harmonic oscillator single-particle wave functions with $\hbar\omega = 12.65$ MeV [5]. Those wave functions are also used for the initial ${}^6\text{Li}$ state to obtain the halo result with the final ${}^6\text{He}$ state being specified by WS wave functions in the $0p$ -shell and higher orbitals only as given in the halo calculation of the scattering presented above. Such a specification introduces a problem in normalization with the $0p_{\frac{3}{2}}$ wave functions. The overlap of the HO and WS $0p_{\frac{3}{2}}$ radial wave functions is 0.96, hence the wave functions preserve the norm to within 4%. Both results are compared to the data of Shaw *et al.* [33] (circles) and Shoda *et al.* [34] (squares) in Fig. 8, wherein the halo and non-halo calculations are displayed by the dashed and solid lines respectively. From the available data one may infer that the non-halo result is favored, but this is due to the datum at 137° only. Note that our non-halo result is similar to that found by Doyle *et al.* [35] in which they used a $0\hbar\omega$ model of structure and no specific halo structure was specified. Our halo result is very similar to the result obtained from a three-body description of ${}^6\text{He}$ in which the wave functions reproduced the halo properties [36]. More data in the region of the possible minimum as well as at large angles are needed to confirm the conjecture that ${}^6\text{He}$ does not have a halo structure.

IV. CONCLUSIONS

The available scattering data from hydrogen confirm that ${}^{11}\text{Li}$ is a halo nucleus, while the analysis of the scattering data correctly determines that both ${}^8\text{He}$ and ${}^9\text{Li}$ are not. This confirms our ability to predict correctly any halo structures as probed by the scattering of exotic nuclei from hydrogen. The low-angle scattering results also suggest that ${}^8\text{He}$ is a neutron skin nucleus, as found from breakup reactions.

While the data on the r.m.s. radii suggests that ${}^6\text{He}$ is a halo nucleus, the available scattering data for ${}^6\text{He}$ from hydrogen are not extensive enough to discriminate between the halo and non-halo scenarios; in the measured region they suggest for ${}^6\text{He}$ a very similar matter distribution compared to ${}^6\text{Li}$. The complementary ${}^6\text{Li}(\gamma, \pi^+){}^6\text{He}$ reaction data suggest the non-halo hypothesis. However, it must be stressed that more data, particularly involving transitions to states in ${}^6\text{He}$, are required to support or refute this conjecture.

The analysis presented here also demonstrates that, to test structure models of these exotic nuclei most intensively, one should study reactions of skin and halo nuclei with complementary probes and in complementary reaction channels.

Financial support from the Natural Sciences and Engineering Research Council of Canada, the Australian Research Council, and Department of Energy Grant no. DE-FG02-95ER-40907 is gratefully acknowledged.

REFERENCES

- [1] P. G. Hansen, A. S. Jensen, and B. Jonson, *Ann. Rev. Nucl. Part. Sci.* **45**, 591 (1995).
- [2] D. Aleksandrov, *et al.*, *Nucl. Phys.* **A633**, 234 (1998).
- [3] P. G. Hansen, *Phys. Rev. Lett.* **77**, 1016 (1996); H. Esbensen, *Phys. Rev. C* **53**, 2007 (1996).
- [4] E. Garrido, D. V. Fedorov, and A. S. Jensen, *Phys. Rev. C* **59**, 1272 (1999).
- [5] S. Karataglidis, B. A. Brown, P. J. Dortmans, and K. Amos, *Phys. Rev. C* **55**, 2826 (1997).
- [6] A. A. Korshennikov, *et al.*, *Nucl. Phys.* **A617**, 45 (1997).
- [7] S. Karataglidis and C. Bennhold, *Phys. Rev. Lett.* **80**, 1614 (1998).
- [8] R. Crespo, J. A. Tostevin, and I. J. Thompson, *Phys. Rev. C* **54**, 1867 (1996).
- [9] P. Navrátil and B. R. Barrett, *Phys. Rev. C* **54**, 2986 (1996).
- [10] P. Navrátil and B. R. Barrett, *Phys. Rev. C* **57**, 3119 (1998).
- [11] S. Karataglidis, P. G. Hansen, B. A. Brown, K. Amos, and P. J. Dortmans, *Phys. Rev. Lett.* **79**, 1447 (1997).
- [12] D. C. Zheng, B. R. Barrett, J. P. Vary, W. C. Haxton, and C.-L. Song, *Phys. Rev. C* **52**, 2488 (1995).
- [13] E. K. Warburton and B. A. Brown, *Phys. Rev. C* **46**, 923 (1992).
- [14] OXBASH-MSU (the Oxford-Buenos-Aries-Michigan State University shell model code). A. Etchegoyen, W. D. M. Rae, and N. S. Godwin (MSU version by B. A. Brown, 1986); B. A. Brown, A. Etchegoyen, and W. D. M. Rae, MSUCL Report Number 524 (1986) (unpublished).
- [15] B. S. Pudliner, V. R. Pandharipande, J. Carlson, Steven C. Piper, and R. B. Wiringa, *Phys. Rev. C* **56**, 1720 (1997).
- [16] J. Jänecke, *et al.*, *Phys. Rev. C* **54**, 1070 (1996).
- [17] F. Ajzenberg-Selove, *Nucl. Phys.* **A490**, 1 (1988).
- [18] R. B. Wiringa, *Nucl. Phys.* **A631**, 70c (1998).
- [19] M. G. Gornov, Yu. Gurov, S. Lapshikin, P. Morokhov, V. Pechkurov, T. K. Pedlar, Kamal K. Seth, J. Wise, and D. Zhao, *Phys. Rev. Lett.* **81**, 4325 (1998).
- [20] P. J. Dortmans, K. Amos, S. Karataglidis, and J. Raynal, *Phys. Rev. C* **58**, 2249 (1998).
- [21] M. Lacombe, B. Loiseau, J. M. Richard, R. Vinh Mau, J. Côté, P. Pirès, and R. de Tourreil, *Phys. Rev. C* **21**, 861 (1980).
- [22] F. Ajzenberg-Selove, *Nucl. Phys.* **A506**, 1 (1990).
- [23] P. J. Dortmans, K. Amos, and S. Karataglidis, *J. Phys. G* **23**, 183 (1997).
- [24] D. J. Millener, J. W. Olness, E. K. Warburton, and S. S. Hanna, *Phys. Rev. C* **28**, 497 (1983).
- [25] J. A. Tostevin and J. S. Al-Khalili, *Nucl. Phys.* **A616**, 418c (1997).
- [26] J. S. Al-Khalili, J. A. Tostevin, and I. J. Thompson, *Phys. Rev. C* **54**, 1843 (1996).
- [27] J. S. Al-Khalili and J. A. Tostevin, *Phys. Rev. C* **57**, 1846 (1998).
- [28] P. J. Dortmans and K. Amos, *Phys. Rev. C* **49**, 1309 (1994).
- [29] J. Raynal, computer code DWBA91 (NEA1209/02).
- [30] A. A. Korshennikov, *et al.*, *Phys. Lett.* **316B**, 38 (1993).
- [31] C.-B. Moon, *et al.*, *Phys. Lett.* **297B**, 39 (1992).
- [32] L. Tiator and L.E. Wright, *Phys. Rev. C* **30**, 989 (1984).

- [33] J. Shaw, T. Kobayashi, W. Clayton, L. Ghedira, D. Myers, P. Stoler, P. K. Teng, E. J. Winhold, and J. H. J. Distelbrink, *Phys. Rev. C* **43**, 1800 (1991).
- [34] K. Shoda, O. Sasaki, and T. Kohmura, *Phys. Lett.* **101B**, 124 (1981).
- [35] B. C. Doyle, Nimai C. Mukhopadhyay, and R. S. Wittman, *Phys. Rev. C* **52**, 1957 (1995).
- [36] R. A. Eramzhyan, G. G. Ryzhikh, and Yu. M. Tchuvilsky, *Phys. Atomic Nuclei* **62**, 37 (1999).

TABLES

TABLE I. Root-mean-square (r.m.s.) radii in fm for ${}^6\text{He}$, ${}^8\text{He}$, ${}^9\text{Li}$, and ${}^{11}\text{Li}$. The results of our shell model calculations are compared to those obtained from a Glauber model analysis of the reaction cross sections [26,25], and also from a few-body model analysis of scattering data from hydrogen [2].

Nucleus	<i>r</i> _{r.m.s.}		
	non-halo	halo	Glauber model
${}^6\text{He}$	2.301	2.586	2.54 ± 0.04
${}^8\text{He}$	2.627	2.946	$2.60^{(a)}$
${}^9\text{Li}$	2.238	2.579	2.30 ± 0.02
${}^{11}\text{Li}$	2.447	2.964	3.53 ± 0.10

(a) Taken from [2].

FIGURES

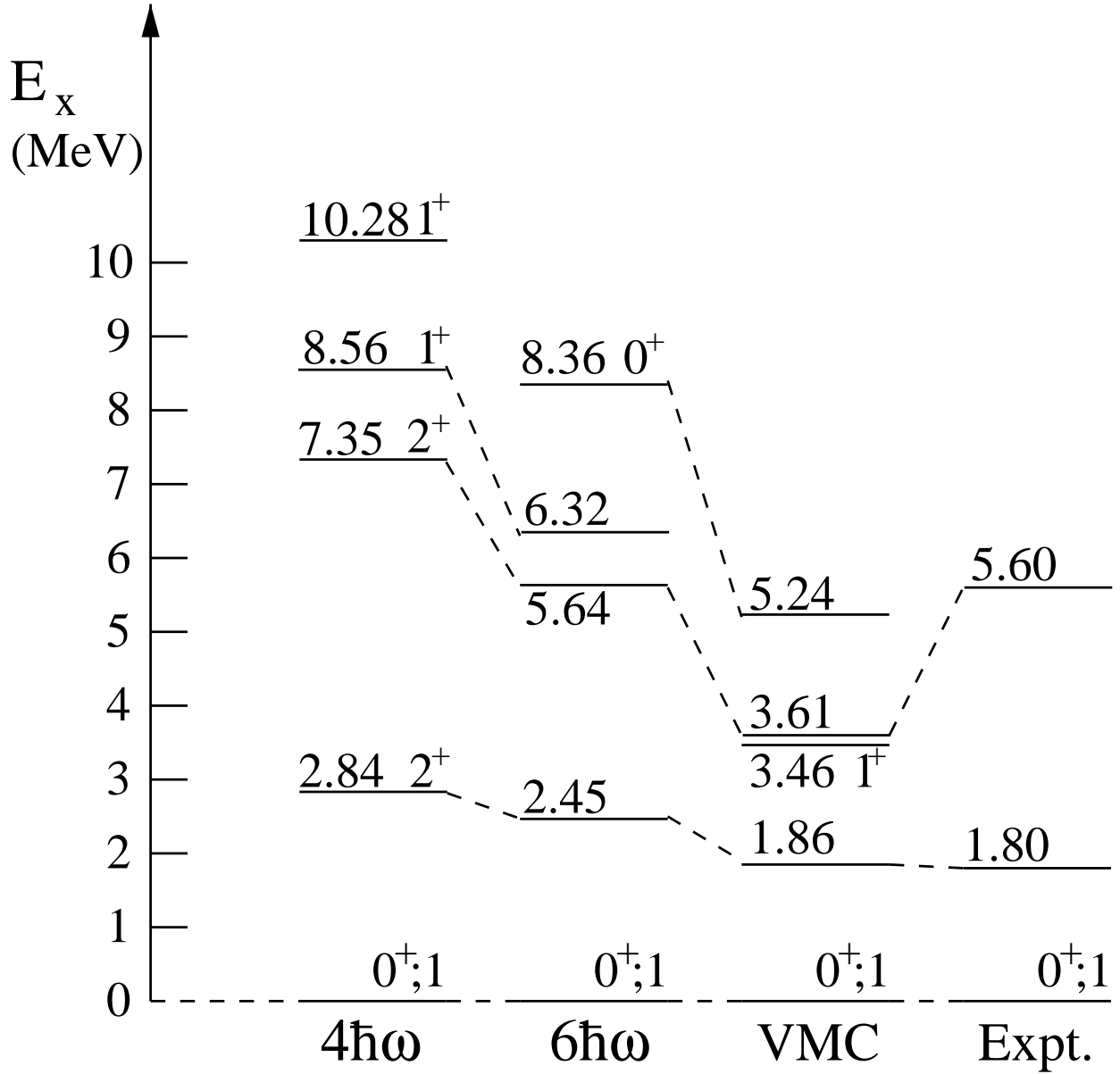


FIG. 1. The spectrum of ${}^6\text{He}$. The result of our $4\hbar\omega$ shell model calculation is compared to that of the $6\hbar\omega$ calculation [9], that of the VMC calculation [15], and to experiment [16].

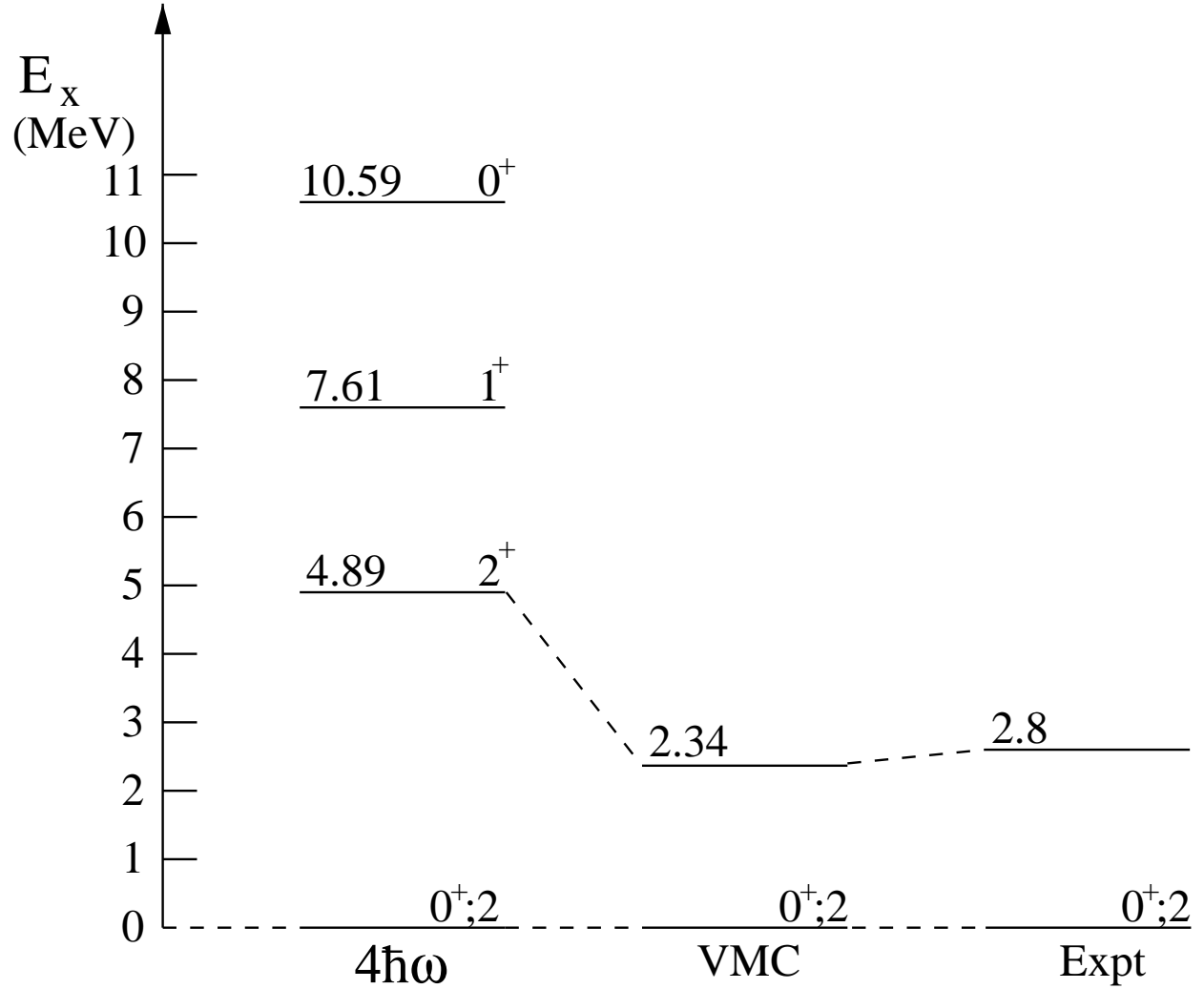


FIG. 2. The spectrum of ${}^8\text{He}$. The result of the present $4\hbar\omega$ shell model calculation is compared to that of the VMC calculation [18]. The data are from Ref. [17].

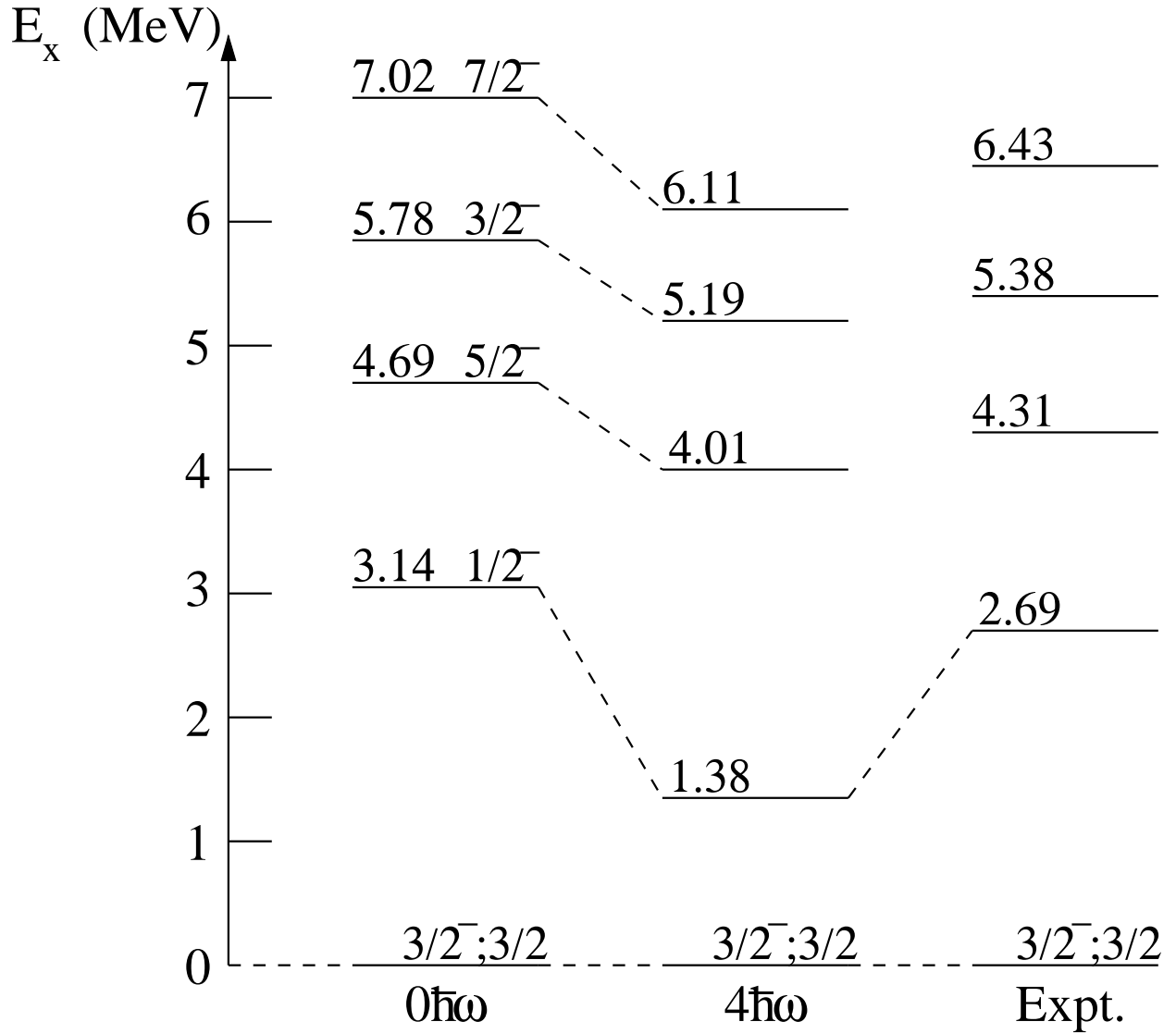


FIG. 3. The spectrum of ${}^9\text{Li}$. The result of the present $0\hbar\omega$ shell model calculation is compared to that obtained in the $4\hbar\omega$ model space [10]. The data are from Ref. [17].

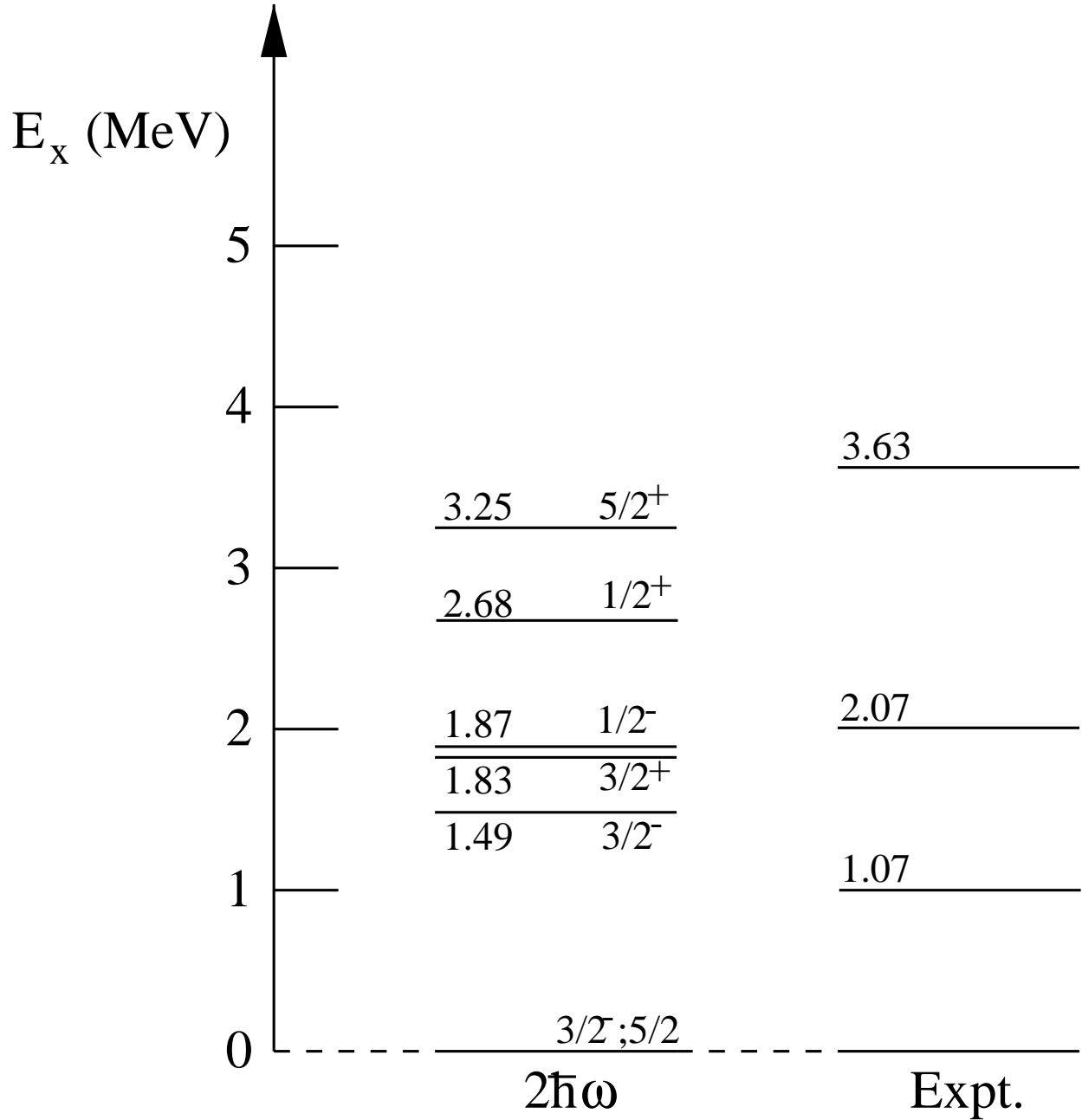


FIG. 4. The spectrum of ^{11}Li . The result of the present $2\hbar\omega$ shell model calculation is compared to the data of Gornov *et al.* [19].

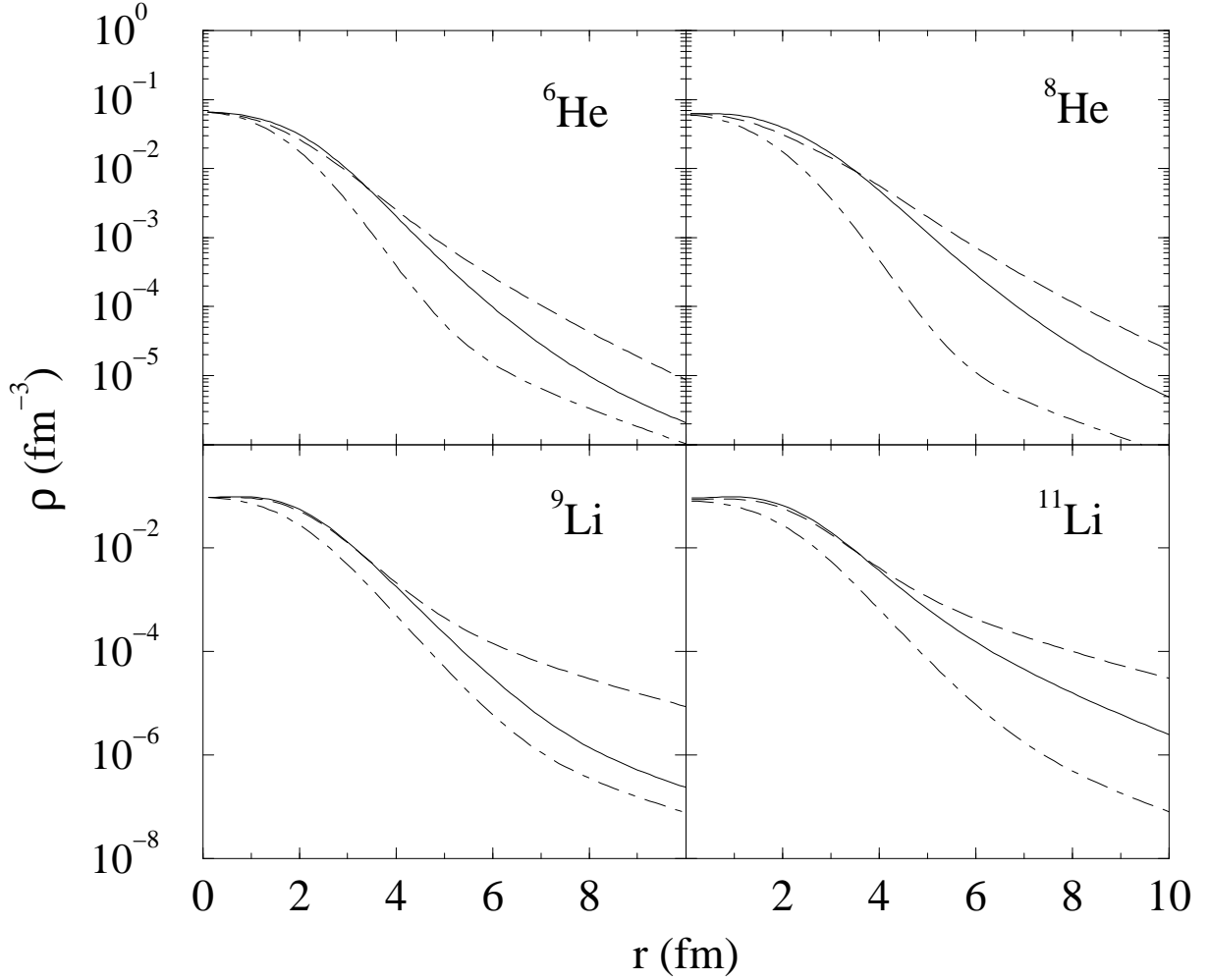


FIG. 5. The (shell model) neutron density profiles for the nuclei ${}^{6,8}\text{He}$ and ${}^{9,11}\text{Li}$. The dashed and solid curves represent, respectively, the profiles when a halo is and is not contained in those structures. The dot-dashed lines represent the proton density for each nucleus.

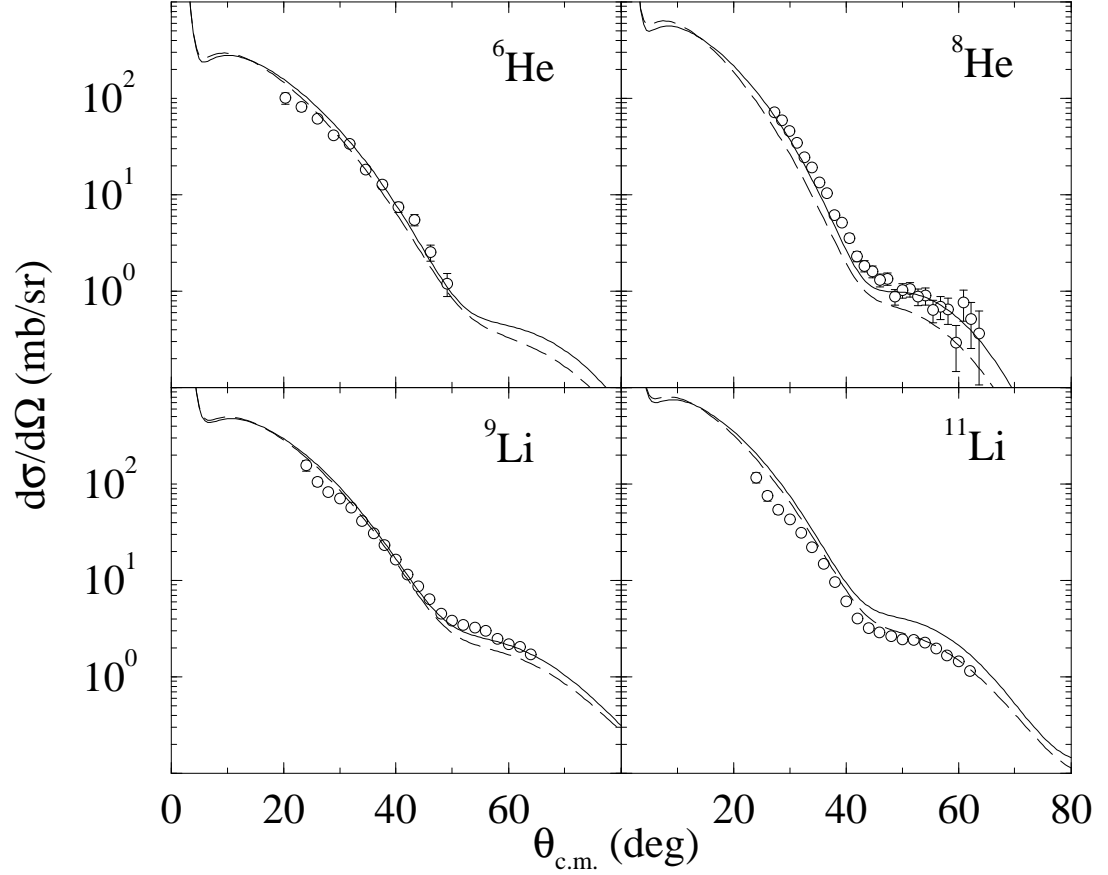


FIG. 6. Predictions of the differential cross sections from the scattering of 72A MeV ${}^6,8\text{He}$ and of 62A MeV ${}^9,11\text{Li}$ from hydrogen compared with experimental data. The data are from Refs. [30,6,31] and the results, assuming that each nucleus has (does not have) a halo structure, are portrayed by the dashed (solid) curves.

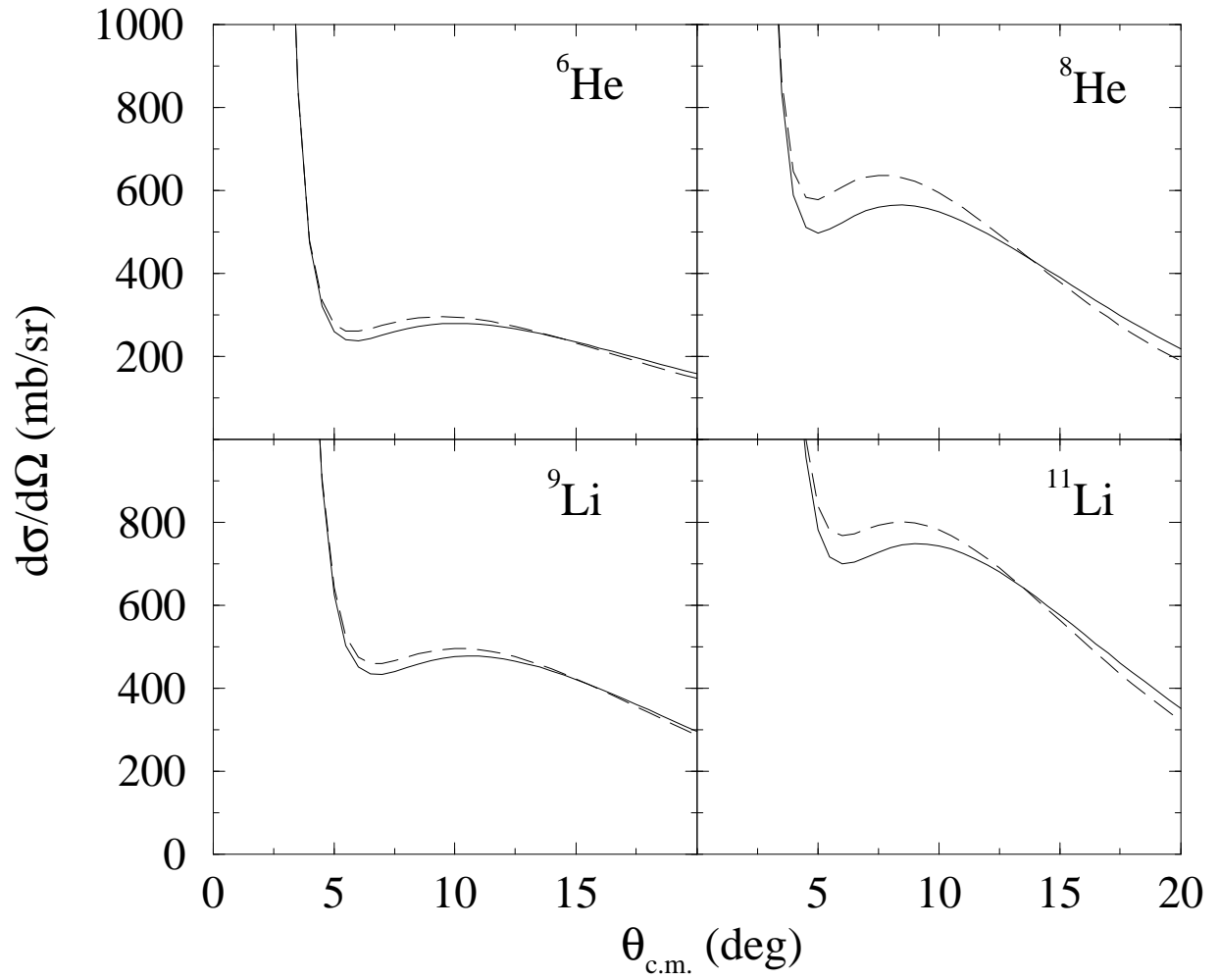


FIG. 7. Differential cross sections as shown in Fig. 6, but for small angles only.

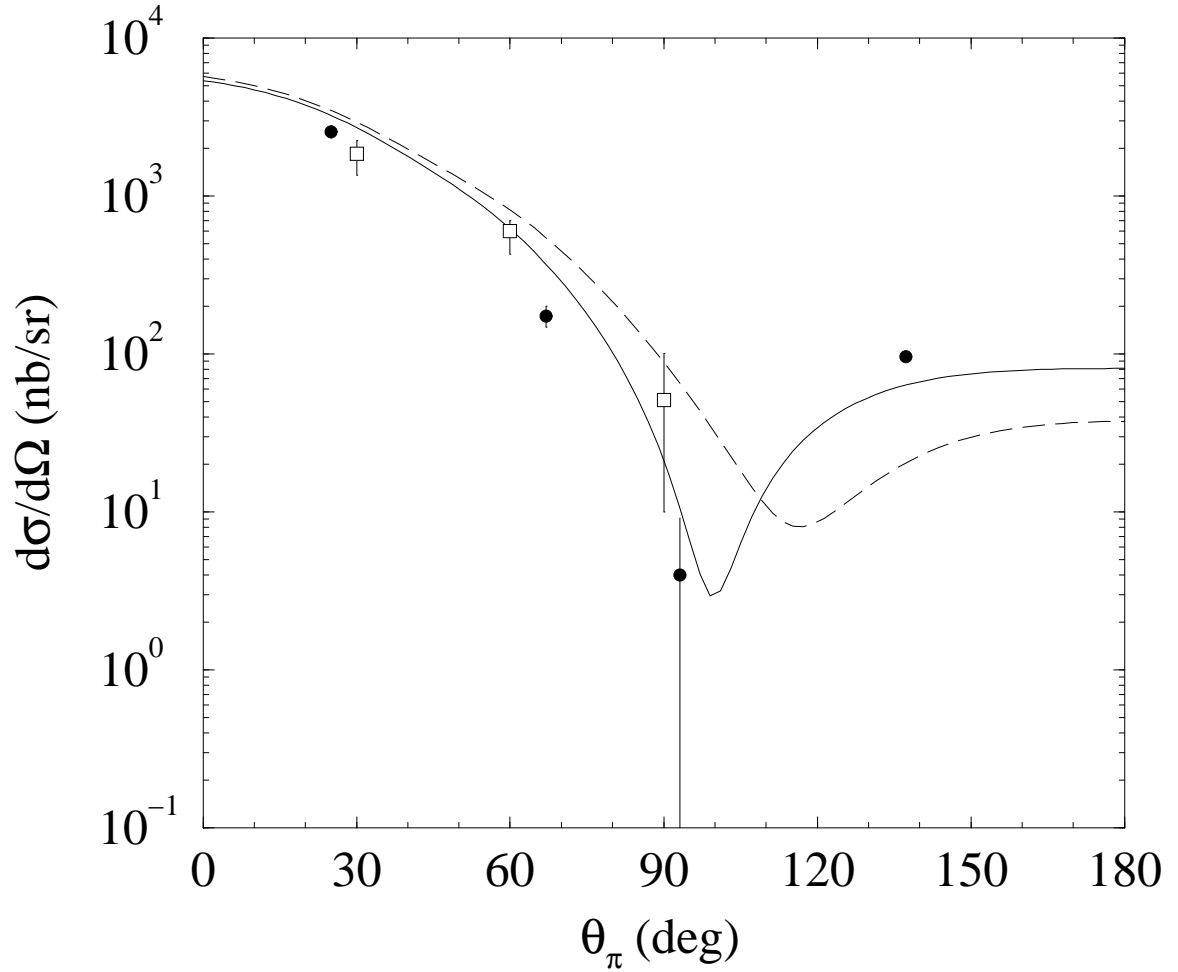


FIG. 8. The ${}^6\text{Li}(\gamma, \pi^+){}^6\text{He}$ reaction for $E_\gamma = 200$ MeV. The data of Shaw *et al.* (circles) [33] and Shoda *et al.* [34] (squares) are compared to the results with and without halo as displayed by the dashed and solid lines.